# The Effects of Age on Lens Transport

Junyuan Gao, Huan Wang, Xiurong Sun, Kulandaiappan Varadaraj, Leping Li, Thomas W. White, and Richard T. Mathias

Department of Physiology & Biophysics, SUNY at Stony Brook, Stony Brook, New York

Correspondence: Richard T. Mathias, Department of Physiology & Biophysics, SUNY at Stony Brook, Stony Brook, NY 11794-8661; richard.mathias@sunysb.edu.

Submitted: June 12, 2013
Accepted: September 11, 2013

Citation: Gao J, Wang H, Sun X, et al. The effects of age on lens transport. *Invest Ophthalmol Vis Sci*. 2013;54:7174–7187. DOI: 10.1167/iovs.13-12593

**Purpose.** Age-related nuclear cataracts involve denaturation and aggregation of intracellular proteins. We have documented age-dependent changes in membrane transport in the mouse lens to see what might initiate changes in the intracellular milieu.

**Methods.** Microelectrode-based intracellular impedance studies of intact lenses were used to determine gap junction coupling conductance, fiber and surface cell membrane conductances, effective extracellular resistivity, and intracellular voltage. Fiber cell connexin expression was detected by Western blotting. Intracellular hydrostatic pressure was measured with a microelectrode/manometer system. Concentrations of intracellular sodium and calcium were measured by intracellular injection of sodium-binding benzofuran isophthalate and Fura2, respectively.

**Results.** In adult lenses, as age increased: fiber cell gap junction coupling conductance declined significantly, correlating with decreases in Cx46 and Cx50 labeling in Western blots; fiber and surface cell membrane conductances did not change systematically; effective extracellular resistivity increased monotonically; center to surface gradients for intracellular pressure, sodium, calcium, and voltage all increased, but in an interdependent manner that moderated changes. In newborn pup lenses, there were changes that did not simply fit with the above paradigm.

**Conclusions.** In newborn pup lenses, the observed changes may relate to growth factors that are not related to age-dependent changes seen in adult lenses. The major change in adult lenses was an age-dependent decrease in gap junction coupling, probably due to oxidative damage leading to degradation of connexin proteins. These changes clearly lead to compromise of intracellular homeostasis and may be a causal factor in age-related nuclear cataracts.

Keywords: lens size, resting voltage, gap junction coupling conductance, intracellular hydrostatic pressure, membrane water permeability, membrane conductance, intracellular sodium concentration, intracellular calcium concentration

Cataract is the leading cause of blindness in the world today.[1] Some cataracts are caused by mutations in genes for lens proteins,[2–4] others are caused by damage to lens proteins through excessive exposure to oxidative agents or UV radiation,[5,6] but the most common cause is simply age. As the lens ages, the intracellular milieu gradually changes: cytoplasmic proteins (the crystallins) accumulate oxidative damage, denature, aggregate, and come out of solution. As a result, old lenses become less compliant (presbyopia) and less transparent (cataracts). These age-related changes begin at the center of the lens and expand outward to eventually form the "age-related nuclear cataract."

The age-related cataract is a dense central opacity that arises because intracellular proteins (crystallins) aggregate and form light-scattering centers. The cataract is associated with extensive oxidative damage to nuclear proteins (reviewed in Spector[5]). This has led to the hypothesis that oxidation might be causal[7] and further hypotheses that specific oxidizing agents such as UV-A radiation,[6,8] $H_2O_2$,[5,9–11] or $O_2$[12–14] could be the causal factor.

However, oxidative damage, at least in young lenses, is prevented by a number of powerful scavenger systems and chaperone molecules (reviewed in Spector[5] and Bron et al.[15]). The scavenger systems include superoxide dismutase, catalase, glutathione reductase, and glutathione peroxidase-1 (GPX-1). Chaperone activity of the α-crystallins was first demonstrated by Horwitz.[16] These crystallins are capable of refolding partially denatured proteins and preventing their aggregation. Lastly, molecular $O_2$ is consumed by mitochondria and other systems,[12] keeping its concentration near zero in the central fiber cells of normal lenses. These systems would need to be compromised in order to get the extensive oxidative damage seen in the age-related cataract. This leads to the question of whether oxidative damage is causal or consequent to some other changes that led to loss of homeostasis. Cataractous lenses also have elevated concentrations of internal $Na^+$ and $Ca^{2+}$, leading several investigators to suggest that $Ca^{2+}$ could be the causal factor.[17,18] However, this hypothesis still lacks the initial step that leads to loss of $Ca^{2+}$ homeostasis.

The lens is a unique organ, formed through continuous cell proliferation and differentiation.[19] Figure 1 illustrates some of the cell variations in the mouse lens. The epithelial cells (E red) vary in shape,[20] cell cycle,[21] and expression of transport proteins[22] from the anterior pole to the equator. At the equator, they undergo dramatic changes in cytoplasmic and membrane protein expression as they begin to elongate and form

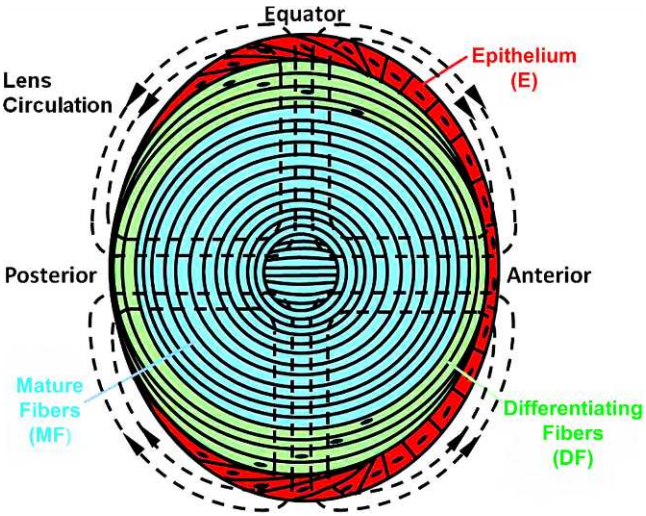


FIGURE 1. A sketch of the various cell types comprising the mammalian lens with the lens internal circulation of salt and water superimposed as dashed lines.

differentiating fibers (DF, green). Signaling and transport by DF also vary from both poles to the equator.[23–25] The DF have intracellular organelles, but at the transition to mature fibers (MF blue), the organelles are degraded[26] and most membrane proteins undergo significant cleavage.[27,28] The overall picture is one of complex spatial localization of biochemical, signaling, and transport properties (reviewed in Mathias et al.[29,30]). One purpose of spatial localization of transport is to generate an internal microcirculatory system, which is critical for homeostasis of the MF (reviewed in Mathias et al.[29]).

The pattern of the circulation is shown by the dashed lines of flow superimposed on the sketch of the lens in Figure 1. The circulating current is carried primarily by sodium, which enters the lens along extracellular spaces between cells at the anterior and posterior poles.[22,31,32] As the extracellular $Na^+$ flows toward the center of the lens, it continuously moves down its transmembrane electrochemical potential to enter fiber cells, where it reverses direction to flow back toward the lens surface. Gap junction coupling of fiber cells directs the intracellular flow to the equatorial epithelial cells,[23–25] where the Na/K ATPase is concentrated[22,33,34] to transport the sodium out of the lens. This circulation of salt is followed by a circulation of fluid,[31,35–37] which comprises an internal microcirculatory system that delivers nutrients and antioxidants to central fiber cells of the lens.[38–42]

Compromise of this microcirculatory system leads to loss of homeostasis in central fiber cells and a central cataract.[43–46] The purpose of the current study was to determine if age causes the lens circulation to deteriorate, which could be a major factor in the onset age-related nuclear cataract.

## Materials and Methods

Prior to experimentation, mice were euthanized in accordance with the ARVO statement for The Use of Animals in Ophthalmic and Vision Research. The eyes were removed and placed in a Sylgard-lined Petri dish filled with solution containing (in mM) NaCl 137.7, NaOH 2.3, KCl 5.4, $CaCl_2$ 2, $MgCl_2$ 1, HEPES 5, glucose 10, pH 7.4 (normal Tyrode). The lens, its zonules, and a uveal sclera ring of tissue were dissected from the eye. Each lens was pinned by its sclera to the bottom of a chamber with a Sylgard base. The chamber was mounted on the stage of a microscope and perfused with a normal Tyrode solution. All studies were performed on lenses from mice of C57 Black or mixed C57/J129 genetic backgrounds.

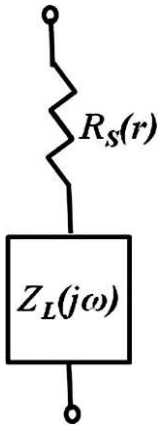


FIGURE 2. An equivalent circuit representation of the lens impedance. Explicit definitions of $R_S$ and $Z_L(j\omega)$ are given in the text.

## Intracellular Impedance

Impedance of intact lenses was measured as described in Gao et al.[47] Briefly, a centrally placed intracellular microelectrode injected a stochastic current composed of sinusoidal frequencies between 0 Hz and 5 KHz. A peripherally placed intracellular microelectrode recorded the induced voltage. Both signals were sent to a fast Fourier analyzer (Hewlett Packard, Palo Alto, CA) where the intracellular impedance was calculated in real time. Figure 2 illustrates a structurally based equivalent circuit model of the lens, (Fig. 2) $Z(j\omega)$,[47–49] which was used to curve fit the data and obtain estimates of the membrane conductances of surface cells and internal fiber cells, and the effective resistivity of the extracellular spaces within the lens. The series resistance, $R_S$, arises because of the intracellular microelectrode point source of current at the lens center. The injected current has two pathways to leave the lens: it can flow intracellularly to the lens surface where it leaves the lens through the admittance of surface cell membranes, $Y_S$; or it can take a parallel path, crossing fiber cell membranes to enter the extracellular space within the lens, where it flows to the lens surface through the distributed admittance $Y_e$.

$$Z(j\omega) = R_S(r) + Z_L(j\omega)$$

$$Z_L(j\omega) = \frac{1}{4\pi a^2 (Y_S[j\omega] + Y_e[j\omega])} \quad (1)$$

$$Y_S(j\omega) = G_S + j\omega C_S$$

$$Y_e(j\omega) = \frac{\gamma}{R_e}\left(\coth\gamma a - \frac{1}{\gamma a}\right), \gamma = \sqrt{R_e \frac{S_m}{V_T}(g_m + j\omega c_m)}$$

$G_S$ and $g_m$ (S/cm$^2$) are respectively surface and fiber cell membrane conductances, $C_S$ and $c_m$ ($F$/cm$^2$) are respectively surface and fiber cell membrane capacitances, $R_e$ (Ωcm) is the effective resistivity of the extracellular spaces within the lens, $a$ (cm) is the lens' radius, and $S_m/V_T$ (cm$^{-1}$) is the average surface area of fiber cell membrane per volume of tissue. The parameter $j = \sqrt{-1}$, and ω represents an arbitrary sinusoidal frequency.

The series resistance ($R_S$ $K\Omega$) is defined as the high frequency asymptote of the magnitude of the impedance. It has been shown to be directly proportional to the resistance of gap junctions between the point of voltage recording and the lens surface.[49] By advancing the microelectrode along its track toward the lens center, the series resistance at several depths in each lens was recorded and similar data pooled from several lenses to determine gap junction coupling conductance. The relationship between resistance $R_S$ ($r$) and underlying effective intracellular resistivities ($R_{DF}$ and $R_{MF}$ $\Omega$cm) has two forms, depending on whether one is recording in the outer DF or inner mature fibers (MF):

$$R_S(r) = \begin{cases} \dfrac{R_{DF}}{4\pi a}\left(\dfrac{1}{r/a} - 1\right) & b \le r \le a \\ \dfrac{R_{DF}}{4\pi a}\left(\dfrac{1}{b/a} - 1\right) + \dfrac{R_{MF}}{4\pi a}\left(\dfrac{1}{r/a} - \dfrac{1}{b/a}\right) & 0 \le r \le b \end{cases} \quad (2)$$

Equation 2 was derived for current flow in a conductive sphere with a point source of current at its center, hence the $1/r$ dependence, where $r$ is the distance from the lens center and $a$ is the lens radius. In mouse lenses, the location $r = b$ ($b \approx 0.85a$) is the transition between DF ($r \ge b$), which have organelles, and MF ($r \le b$), which lack organelles.[30] It is also the site of extensive posttranslational modification of fiber cell membrane proteins, including the connexins. As a consequence, $R_{DF}$ is generally less than $R_{MF}$ and there is a change in the slope of the series resistance versus location curve at $r = b$. The cell-to-cell conductance per area of fiber cell contact (S/cm$^2$) is estimated from $G_{DF} = 1/(R_{DF}w)$, $G_{MF} = 1/(R_{MF}w)$, where $w = 3 \times 10^{-4}$ cm is the average width of a fiber cell.

## Western Blotting

Lenses from 11-week or 11-month-old mice were dissected and their diameters were measured and used to calculate lens volume. Dissected lenses were homogenized in 0.1 M NaCl, 0.1 M $Na_2HPO_4$, 10 mM ascorbic acid, and protease inhibitors (10 μg/mL each of chymostatin, leupeptin, and pepstatin). After centrifugation at 14,000$g$ for 20 minutes at room temperature, the insoluble fraction was subjected to a second wash with 1 mL of 0.1 M NaCl, 0.1 M $Na_2HPO_4$, followed by a subsequent wash with 1 mL of 20 mM NaOH. The insoluble fraction was finally washed in 1 mL of 1 mM $Na_2CO_3$, after which the pellets were resuspended in a volume of sample buffer proportional to the total starting lens volume and stored at −80°C. Equal volumes of samples from each age were electrophoresed on 10% SDS-polyacrylamide gels and transferred to nitrocellulose membranes (GE Healthcare Bio-Sciences, Pittsburg, PA). Commercial protein standards (MagicMark; Invitrogen, Carlsbad, CA) were used as molecular weight markers. Blots were then probed with antibodies specific for the carboxy tail of Cx46 (rabbit[50]), the cytoplasmic loop of Cx50 (goat; Santa Cruz Biotechnology, Santa Cruz, CA), or α-tubulin (mouse, provided by Dr I. Spector, Stony Brook University). Horseradish peroxidase-conjugated goat anti-rabbit, rabbit anti-goat, (Jackson ImmunoResearch, West Grove, PA), or sheep anti-mouse (GE Healthcare Bio-Sciences) secondary antibodies were used prior to enhanced chemiluminescence detection. Blots were visualized and band intensities were quantified using a commercial imager and software (FluorChem E and AlphaView; Protein Simple, Santa Clara, CA). Western blots of lenses from three mice each, at ages of 2 and 16 months, were compared (data not shown) and blots of lenses from three mice each, at ages of 11 weeks and 11 months were compared (see Results). Both studies showed reductions in labeling that were consistent with reductions in gap junction coupling conductance, but the 11-week versus 11-month blots had the advantage of using α-tubulin as a control for nonspecific reductions in labeling.

## Intracellular Hydrostatic Pressure

Intracellular hydrostatic pressures in intact lenses were measured as described in Gao et al.,[36] so only a brief description is given here. A microelectrode was filled with 3 M KCl, and its resistance (1.5–2.0 MΩ) was recorded in solution outside of the lens. The electrode was then inserted into the lens, where positive intracellular pressure pushed cytoplasm into the tip, causing the resistance to increase. A side port on the electrode holder was connected by plastic tubing to a mercury manometer, which allowed adjustment of the pressure within the electrode. When pressure within the electrode was equal to intracellular pressure, cytoplasm was just pushed out of the electrode and the electrode resistance returned to its original value measured in the bathing solution. This was the recorded value of intracellular pressure.

Intracellular pressures were recorded at four to five different depths in each lens. The recordings were made along a track that started at the surface, 45° between the posterior pole and equator, and led to the lens center. The position of the tip of the microelectrode was recorded at each location where the pressure was measured. The data from 6 to 10 lenses were pooled.

## Intracellular Sodium and Calcium

The intracellular concentrations of sodium and calcium were measured using a dual wavelength spectrometer system as described in Wang et al.[45] To measure sodium, sodium-binding benzofuran isophthalate (SBFI, 0.2 mM) was dissolved in the pipette solution. To measure calcium, Fura2 (2 mM) was dissolved in the pipette solution. These solutions were injected into fiber cells at different depths in the lens by advancing the microelectrode along its track toward the lens center. The ratios of emission at 360-/380-nm excitation were compared with calibration curves that were determined at seven depths into the lens. The ratios versus intracellular sodium or calcium concentrations were determined with Equation 3,

$$R = \frac{K_d R_{min} + [X]_i R_{max}}{K_d + [X]_i} \quad (3)$$

where $X$ is either $Na^+$ or $Ca^{2+}$, $R$ is the experimentally measured ratio at a given depth in the lens, whereas the $K_d$s, $R_{min}$s, and $R_{max}$s were determined by the calibration curves at the same depth. The $K_d$s were essentially independent of depth, but the maximum and minimum ratios, $R_{max}$ and $R_{min}$, respectively, varied significantly because the lens absorbs light in a wavelength- and depth-dependent manner.[44]

# Results

The lens grows throughout the lifetime of an organism, so there is an age-dependent increase in size that is expected to change the lens circulation and thus the intracellular milieu. For example, if specific membrane-transport properties remain the same, increased size should cause increases in the intracellular gradients for sodium, calcium, voltage, and hydrostatic pressure.[47] In addition to these predicted changes, aging involves

Glossary

| | | |
|---|---|---|
| $a$ | (cm) | Lens radius. |
| b | ($\approx 0.85a$) | Location of the DF to MF transition. |
| $c_m$ | (F/cm$^2$) | Fiber cell membrane capacitance. |
| $C_s$ | (F/cm$^2$) | Surface cell membrane capacitance. |
| DF | ( - ) | Differentiating fibers. |
| $e$ | (subscript) | Extracellular in the lens. |
| $E_{Na}$ | (Volts) | Sodium Nernst potential. |
| F | ($10^5$ coul/mole) | Faraday constant. |
| $g_m$ | (S/cm$^2$) | Fiber cell membrane conductance. |
| $G_S$ | (S/cm$^2$) | Surface cell membrane conductance. |
| $i$ | (subscript) | Intracellular. |
| $j_{Na}$ | (moles/cm$^2$s) | Average membrane $Na^+$ flux into fiber cells. |
| $L_{DF}$ | ((cm$^3$/s)/mm Hg) | Single gap junction channel hydraulic conductance in DF. |
| $L_{MF}$ | ((cm$^3$/s)/mm Hg) | Single gap junction channel hydraulic conductance in MF. |
| MF | ( - ) | Mature fibers. |
| $N_{DF}$ | (cm$^{-2}$) | Density of open DF gap junction channels. |
| $N_{MF}$ | (cm$^{-2}$) | Density of open MF gap junction channels. |
| $p_i$ | (mm Hg) | Intracellular hydrostatic pressure. |
| $r$ | (cm) | Distance from lens center. |
| $R_e$ | ($\Omega$-cm) | Effective extracellular resistivity in the lens. |
| $R_{in}$ | ($\Omega$) | Input resistance of the lens. |
| $R_{DF}$ | ($\Omega$-cm) | Effective intracellular resistivity in the lens DF. |
| $R_{MF}$ | ($\Omega$-cm) | Effective intracellular resistivity in the lens MF. |
| $R_S$ | ($\Omega$) | Series resistance due to fiber gap junctions. |
| $S_m/V_T$ | (cm$^{-1}$) | Surface of fiber cell membrane per volume tissue. |
| $u_i$ | (cm/s) | Intracellular fluid flow. |
| $w$ | ($3 \times 10^{-4}$ cm) | Fiber cell width. |
| $\gamma_{DF}$ | (S) | Average single gap junction channel conductance in DF. |
| $\gamma_{MF}$ | (S) | Average single gap junction channel conductance in MF. |
| $\psi_i$ | (Volts) | Intracellular voltage. |
| $\psi_e$ | (Volts) | Extracellular voltage. |

the accumulation of oxidative damage to transport proteins, in particular fiber cell gap junction channels,[45] which affect all factors involved with the lens circulation.

## The Effects of Age on Fiber Cell Gap Junction Coupling

Figures 3A through D illustrate expanded views of series resistance ($R_S$ K$\Omega$) data versus fractional distance from the lens center ($r/a$), where $r$ (cm) is the actual distance from the center and $a$ (cm) is the lens radius. These data represent the resistance of gap junctions between the point of recording and the surface of the lens. As one looks deeper into the lens, even if the density of gap junctions is constant, the series resistance is cumulative and, because of the spherical geometry, increases as $1/r$. The smooth curves are fits of Equation 2 to the data. Figures 3A through D represent data recorded at the ages of 1 to 3 days, 2, 6, and 14 months, respectively; except for experiments on newborn pup lenses, which were studied almost immediately after birth, all experiments were conducted within a week of these ages.

At the DF to MF transition ($r = 0.85a$, see vertical arrows in Figs. 3A–D), there is a change in slope of the series resistance versus location data. In Figures 3B through D, the slope increases in MF relative to DF, which is a consistent observation in all lenses previously studied.[30,49–52] Contrary to this general decrease in coupling conductance at the DF to MF transition, Figure 3A shows that, in lenses from newborn pups, the slope of the series resistance data is much higher in the DF than MF, implying the coupling conductance of MF is much higher than that of DF.

Figure 3E presents an overlay of series resistance data from lenses at each age. In older lenses (6 and 14 months), the nuclei become very hard and it is nearly impossible to get a microelectrode into central cells, hence the data were recorded at depths no greater than 50% of the distance into these lenses. In younger mouse lenses, data can be recorded all the way to the center, and the data were always well fit with Equation 2, which assumes the MF coupling conductance per area of cell-to-cell contact is uniform. The model curves for older lenses make this assumption. The data are graphed as a function of fractional distance from the lens center ($r/a$). When the data are compared in this manner, Equation 2 shows that the series resistance is expected to be proportional to $1/a$, so the larger the radius $a$ (cm), the smaller the expected value of $R_S(r/a)$, assuming that the coupling conductance per area of cell-to-cell contact is constant with age. From panel E, one can clearly see that this expectation does not hold as $R_S$ at each value of $r/a$ is larger in older/larger lenses, directly indicating a decrease in coupling conductance with age. Figure 3F compares series resistance data graphed as a function of actual distance from the lens center, $r$ (cm).

Table 1 tabulates estimated values of radial coupling conductance per area of cell-to-cell contact for differentiating fibers ($G_{DF}$) and mature fibers ($G_{MF}$) at each age, based on fitting Equation 2 to the series resistance data in Figure 3 (see Methods). Note that $G_{DF} = N_{DF}\gamma_{DF}$, $G_{MF} = N_{MF}\gamma_{MF}$, where $N_{DF/MF}$ (1/cm$^2$) is the number of open gap junction channels per area of cell to cell contact in the DF or MF, and $\gamma_{DF/MF}$ (S) is the average single channel conductance of gap junction channels in the DF or MF. There are no data to suggest the single-channel conductance changes, so the assumption is that changes in conductance reflect changes in the number of open channels. Thus, hydraulic conductivity should change in proportion to ionic conductivity. Table 1 also tabulates the average radius ($a$ $cm$) for these groups of lenses at each age. Gap junction coupling conductance in lenses from newborn pups (aged 3–5 days) is much larger than expected, particularly between mature fibers (see Discussion).

Reductions in coupling conductance could reflect either degradation of connexins or closure of channels that remain

Table 1. A Comparison of the Best Fit Values of Coupling Conductance per Area of Cell-to-Cell Contact in DF and MF From Lenses of Different Ages

| | 3–5 d, $n = 12$ | 2 mo, $n = 12$ | 6 mo, $n = 7$ | 14 mo, $n = 6$ |
|---|---|---|---|---|
| $G_{DF}$, S/cm$^2$ | 1.54 | 0.93 | 0.56 | 0.25 |
| $G_{MF}$, S/cm$^2$ | 27.32 | 0.82 | 0.33 | 0.24 |
| $a$, cm | 0.067 ± 0.004 | 0.110 ± 0.003 | 0.125 ± 0.001 | 0.130 ± 0.003 |

The bottom row gives the average radius for each group of lenses studied.

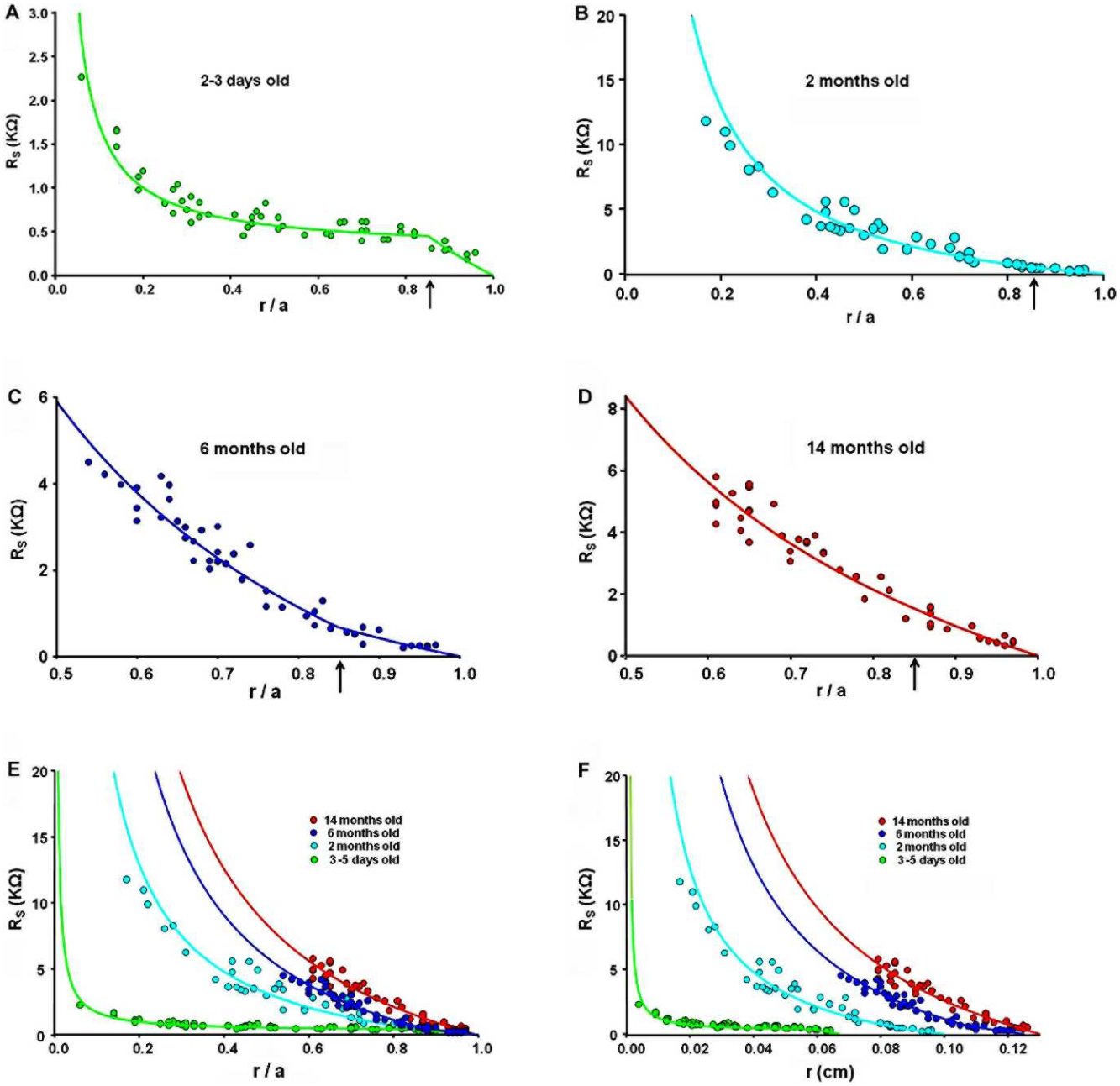


FIGURE 3. A comparison of the series resistance ($R_S$) at different ages. (**A–D**) Expanded plots of the series resistance at the ages indicated, graphed as a function of the fractional distance from the lens center ($r/a$), where $r$ (*cm*) is the actual distance and $a$ (*cm*) is the lens radius. The vertical arrows at $r/a = 0.85$ indicate the assumed location of the DF to MF transition. (**E**) An overlay of the series resistance data at different ages graphed as functions of the fractional distance from the lens center. (**F**) An overlay of the series resistance data graphed as a functions of the actual distance ($r$) from the lens center.

intact. Western blots reported in Wang et al.[45] 2009 suggested oxidative damage led to degradation of connexins, since antibodies to the C-terminus of Cx50, the C-terminus of Cx46 and the cytoplasmic loop of Cx50 all showed reductions in labeling that were comparable with the reduction in conductance. Figure 4 shows Western blots labeling the C-terminus of Cx46 and the cytoplasmic loop of Cx50 protein, each aged at either 11 weeks or 11 months. Since the C-terminus of Cx46 is cleaved in the MF, our antibody only detects Cx46 in the DF, whereas Cx50 is detected in both DF and MF. Age affects essentially every protein in the lens, so there is no standard for normalization of labeling intensity. However, when equal volumes of lens tissue were compared, α-tubulin was found to be the same at 11 weeks and 11 months, though it eventually decreased somewhat by 14 months. The ages of 11 weeks and 11 months were therefore chosen for studying labeling of Cx46 and Cx50, with α-tubulin acting as a control for nonspecific reductions in labeling. There is clearly a very significant reduction in labeling of both Cx46 and Cx50 protein at 11 months in comparison to 11 weeks, with the intensity at 11 months being approximately 51% of that at 11 weeks for either Cx46 or Cx50. These data do not necessarily mean the loss of connexins was due to accumulation of oxidative damage. However, our previous study in which protection from oxidative damage (GPX-1) was knocked out[45] showed the lens fiber cell connexins were very sensitive

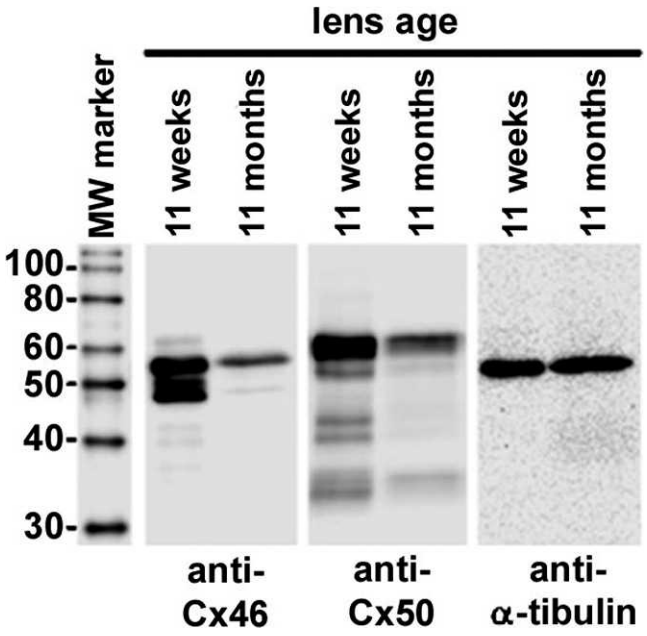


Figure 4. Western blots of lens fiber cell connexins with α-tubulin as a control. Cx46 was detected using an antibody against the C-terminus, which is cleaved in MF so only DF protein is detected. Cx50 was detected with an antibody against the cytoplasmic loop, which is not cleaved in MF so both DF and MF lens protein were detected. In either case, the intensity of the major band at 11 months is 51% of that at 11 weeks for either Cx46 or Cx50. The other bands are probably degradation products. These data, like the gap junction coupling conductance data, suggest a loss of connexin protein with age.

to degradation by oxidative damage. Insofar as accumulation of oxidative damage with age is inescapable, our working hypothesis is that age-dependent accumulation of oxidative damage leads to degradation of lens fiber cell connexins.

## The Effect of Age on Lens Fluid Circulation

The data in Table 1 show $G_{DF}$ and $G_{MF}$ have decreased with age, indicating the number of open gap junction channels has decreased with age. Hydraulic conductivity also depends on the number of open gap junction channels, so it too should have decreased with age in proportion to ionic conductivity. The reduced hydraulic conductivity and increased radius with age should both cause intracellular hydrostatic pressure, $p_i$, to increase with age. This was indeed the case, as seen in Figure 5A, which presents an overlay of intracellular hydrostatic pressures at each age graphed as a function of fractional distance from the lens center. The smooth curves are the best fit of a structurally based model derived in Gao et al.[36] The model curves are basically the mean value of the data at each radial location, whereas the scatter in the data around these curves provides estimates of the standard deviations. The fit of the model was used to estimate the values of $p_i(0)$ and $p_i(b)$ presented in Table 2. Both $p_i(0)$ and $p_i(b)$ monotonically increase with age, but the increase was not as large as expected based on the increases in radii and decreases in the number of open gap junction channels (see Discussion).

Table 2. A Comparison of the Best Fit Values of Central Intracellular Hydrostatic Pressures and Hydrostatic Pressures at the DF to MF Transition Where $r = b$ Measured in Lenses of Different Ages

| | 3–5 d, $n = 6$ | 2 mo, $n = 16$ | 6 mo, $n = 4$ | 14 mo, $n = 8$ |
|---|---|---|---|---|
| $p_i$ (0), mm Hg | 62 | 349 | 433 | 493 |
| $p_i$ (b), mm Hg | 20 | 62 | 77 | 98 |
| $u_i(X$ mo)/$u_i(2$ mo) | 0.86 | 1.00 | 0.66 | 0.36 |

The bottom row presents an estimate of the relative values of average water flow velocity based on Equation 4 and the data in Tables 1 and 2.

Figure 5B presents the same pressure data, but graphed as a function of actual distance from the lens center, $r$ (cm). Pressure driven intracellular water flow velocity at the lens surface, $u_i(a)$ ($cm/s$), is given by:

$$u_i(a) = -wN_{DF}L_{DF}\frac{dp_i(a)}{dr} \quad (4)$$

Though our data do not specify $N_{DF}L_{DF}$, the coupling-conductance data provide estimates of the relative changes in $N_{DF}$ with age, and the pressure versus $r$ data provide estimates of age-dependent changes in the pressure gradient at the lens surface, which was estimated from $p_i(b)/(b - a)$. Relative changes in $u_i(a)$ with age can therefore be directly estimated from the data. The results are presented in Table 2. Water flow velocity, in lenses from adult mice, monotonically decreased as age increased, which explains why the central pressure did not increase as much as expected. However, water flow velocity in lenses from newborn pups decreased relative to that at age 2 months, opposite to the trend in adult lenses (see Discussion).

The circulation of fluid appears to be osmotically generated at the fiber cell membrane by salt influx (primarily sodium) with water following, primarily through the fiber cell

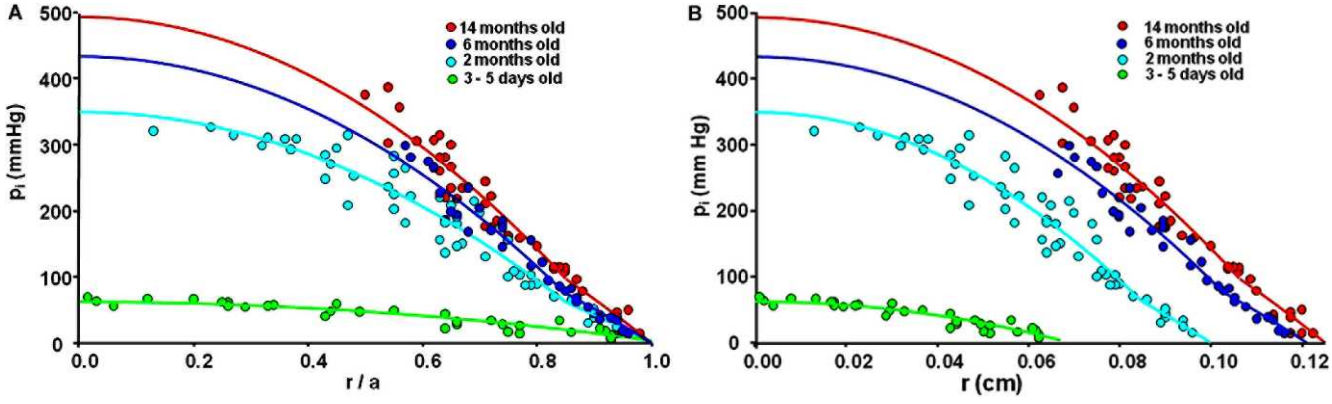


Figure 5. A comparison of intracellular hydrostatic pressures ($p_i$) at different ages. (**A**) The pressures are graphed as a function of the fractional distance from the lens center ($r/a$). (**B**) The pressures are graphed as a function of the actual distance from the lens center ($r$).

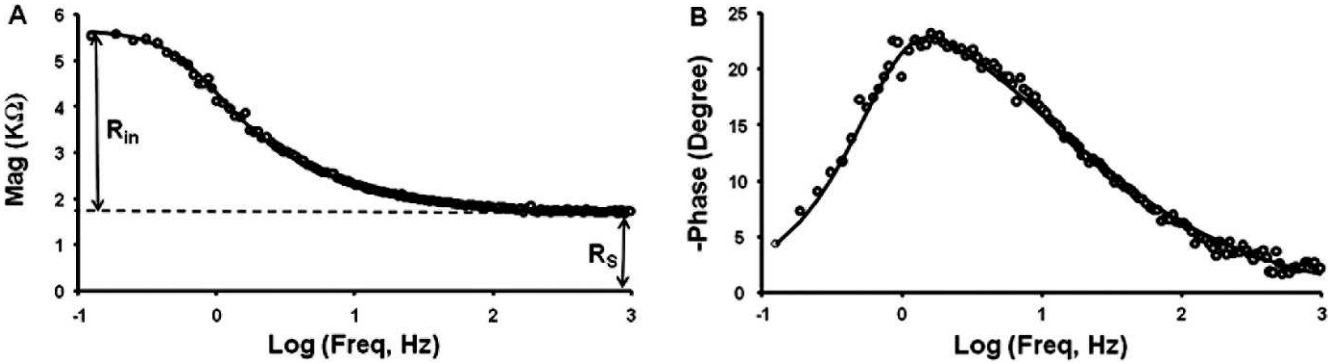


FIGURE 6. Intracellular impedance data from a 2-month-old mouse lens. A. The magnitude of the impedance, which represents the resistance of the lens as a function of sinusoidal frequency. At 0 Hz, the magnitude is the input resistance of the lens ($R_{in}$), whereas at high frequency, the magnitude asymptotes to the series resistance ($R_S$). (**B**) The phase of the impedance, which represents the normalized time delay between the input sinusoidal current and the responding sinusoidal voltage. These data were curve fit with an equivalent circuit model of the lens to determine membrane conductances of fiber cells and surface cells, and the effective extracellular resistivity.[47]

membrane water channel AQP0.[36] Membrane water permeability is quite high relative to salt permeability, so sodium entry is rate limiting and one would not expect changes in membrane water permeability to have much effect, unless it decreased by more than an order of magnitude.[53] Fiber cell membrane water permeability was previously reported in abstract format[54] for membrane vesicles isolated from the DF of lenses from 2-month and 14-month-old mice; it decreased somewhat, going from approximately 35 μm/s to 23 μm/s. Based on calculations in Mathias and Wang,[53] this decrease was not sufficiently large to have contributed to the decreases in $u_i(\alpha)$ reported in Table 2.

## The Effect of Age on Electrical Properties

When a sinusoidal current of frequency $f$ (Hz) is injected into a central fiber cell, the responding intracellular voltage change is a sinusoid of the same frequency, but the amplitude and time-shift are determined by the equivalent circuit properties of the lens. The magnitude of the lens impedance at each frequency is the ratio of the voltage to current amplitudes of the sinusoids, and the phase is the normalized time shift between the current and voltage sinusoids. Figure 6 shows a typical lens impedance response; in this case the data were collected at age 2 months, but data at other ages are similar in terms of the overall frequency response, but with age-dependent changes in amplitude and natural frequency. The smooth curves are the best fit of an equivalent circuit model of the lens (Equation 1).

When recording intracellular impedance, the values of series resistance ($R_S$), radius ($a$), and intracellular voltage ($\psi_i[r]$) were determined. These are model-independent parameters that are directly measured from the data; the value of series resistance is indicated on the magnitude data shown in Figure 6A. The series resistance data were included in the graphs shown in Figure 3, and they were used to estimate the coupling conductances tabulated in Table 1.

The age-dependence of the lens radius is graphed in Figure 7A. The mouse lens radius increased exponentially with age with a best-fit value at birth ($t = 0$) of $a = 0.059$ cm and a final value ($t = \infty$) of $a = 0.129$ cm and a time constant of 49 days.

Figure 7B presents an overlay of intracellular voltages at each age, graphed as a function of fractional distance from the lens center. The data have a lot of scatter, but it is obvious that the voltage becomes progressively more depolarized as lens age/size increases. As the voltage becomes more depolarized with age, the electrochemical potential for sodium to enter fiber cells diminishes. This causes the circulation of sodium to decrease, and should also cause a decrease in the circulation of fluid, as reported in Table 2 for adult lenses. The data were fit with a structurally based model derived in Wang et al.,[45] that specifies the voltage in lens surface cells, $\psi_i(a)$, and the

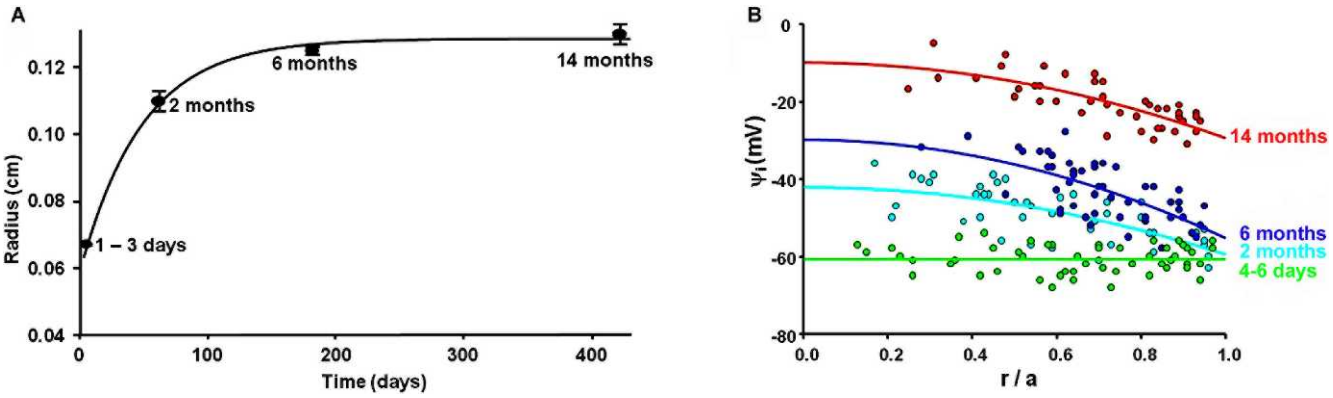


FIGURE 7. The age-dependence of the lens radius and intracellular voltage. (**A**) The radius of mouse lenses increases exponentially with age, from 0.059 cm at birth to a final value of 0.129 cm, with a time constant of 49 days. (**B**) A comparison of the lens intracellular voltages at the various ages indicated, graphed as a function of fractional distance from the lens center.

**Table 3.** A Comparison of Lens Surface Voltage and the Change in Voltage Between the Surface and Center

| | 4–6 d, $n = 10$ | 2 mo, $n = 7$ | 6 mo, $n = 8$ | 14 mo, $n = 6$ |
|---|---|---|---|---|
| $\psi_i(a)$, mV | −61 | −60 | −55 | −29 |
| $\Delta\psi_i$, mV | 0 | 17 | 25 | 19 |
| $j_{Na}$, *pmoles*/cm$^2{}_s$ | ~4–5 | 3.46 | 1.58 | 0.81 |

Equation 5 describes the values of radial gradients for the lens intracellular voltage.

intracellular voltage gradient between the lens center and surface, $\Delta\psi_i$.

Table 3 tabulates the age dependence of $\psi_i(a)$ and $\Delta\psi_i$. Based on model calculations,[45] $\Delta\psi_i$ is given by:

$$\Delta\psi_i = \frac{S_m}{V_T}\frac{a^2}{6}\frac{Fj_{Na}}{wN_{MF}\gamma_{MF}} \quad (5)$$

This equation ignores the small change in the slope of $\psi_i(r)$ *vsr* at $r = b$, since the data were too scattered to detect such a change. The voltage gradient depends directly on the volume averaged sodium current density entering fiber cells of the lens ($Fj_{Na}$), where the Faraday constant $F = 10^5$ coul/mole and $j_{Na}$ *moles/cm$^2$s* is the volume averaged sodium flux into fiber cells. The fiber cell surface of membrane to volume of tissue ratio, $S_m/V_T = 6000$ cm$^{-1}$, and fiber cell width $w = 3 \times 10^{-4}$ cm, are assumed to be approximately constant with age. The values of $a$ and $N_{mF}\gamma_{MF} = G_{MF}$ are tabulated in Table 1 and the values of $\Delta\psi_i$ are tabulated in Table 3, so these values were used to directly estimate $j_{NA}$, which is tabulated in Table 3. The values monotonically decrease with age in a manner that is consistent with the decreases in the fiber cell transmembrane electrochemical potential for sodium with age (see Discussion).

This was an electrical determination of $j_{Na}$, which compares favorably with the predicted changes in $j_{Na}$ determined from hydrostatic pressure in adult lenses or with intracellular water flow velocity in lenses from mice of all ages (see Discussion). However, owing to the enormous coupling conductance of MF in lenses from newborn pups, the value of $\Delta\psi_i$ is essentially zero, hence it provided no quantitative information on $j_{Na}$ in these lenses, other than it is not inordinately large. We assumed it might be 20% to 30% greater in lenses from pups than in lenses from 2-month-old mice, owing to the somewhat larger electrochemical gradient for sodium entry into fiber cells of lenses from pups (note the intracellular voltage is more negative). The values in Table 3 are based on this crude estimate of the change in driving force. Moreover, the reduction in water flow at the surface of newborn pup lenses also provides an estimate of $j_{Na}$ that is in this range.

Figure 8 summarizes the results of curve fitting our equivalent circuit model of the lens (Equation 1) to impedance data recorded at the indicated ages. Figure 8A is the age dependence of the surface cell membrane conductance, $G_S$ ($S/cm^2$), referred to a unit area of lens surface. The surface cell membrane conductance appears to decline significantly between birth and approximately age 2 months, but thereafter it does not change systematically; and given the standard deviations in the data, the time-independent, flat

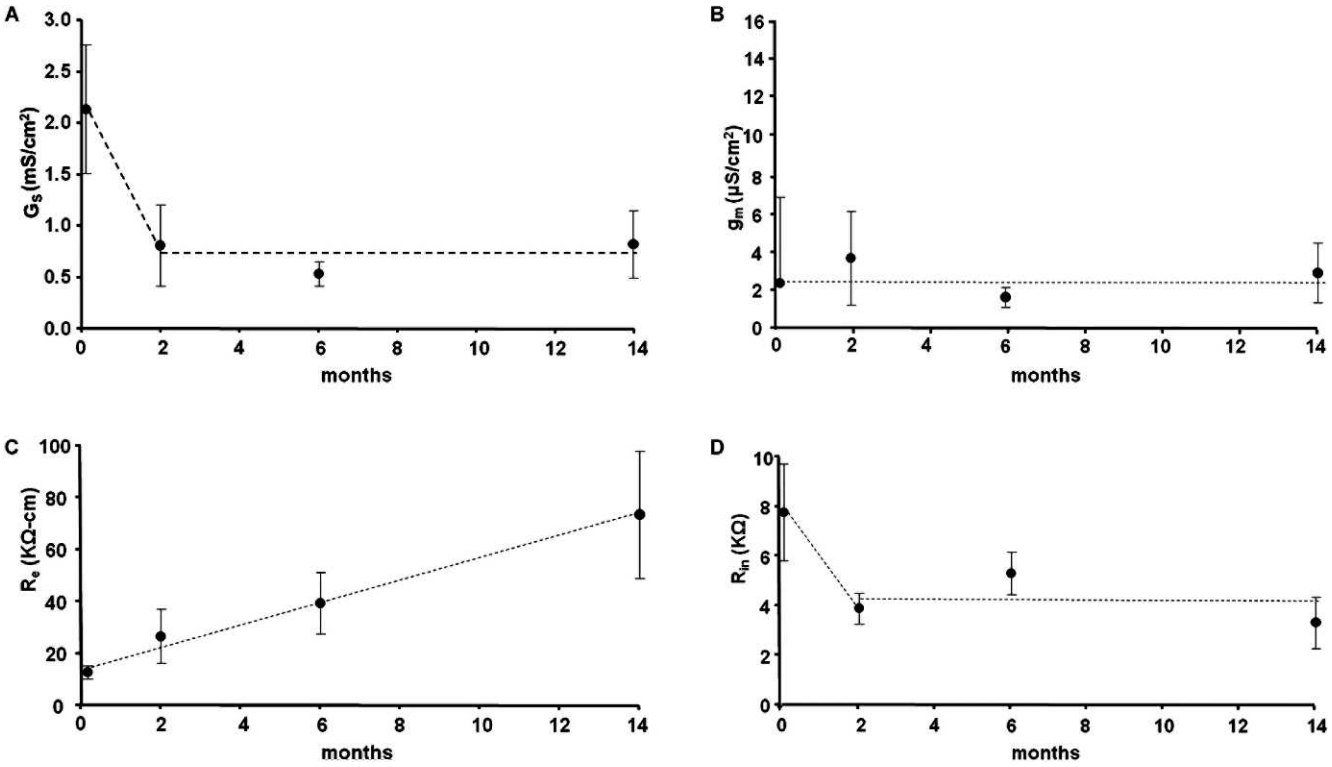


**Figure 8.** The age-dependence of lens membrane conductances and the effective extracellular resistivity determined from curve-fitting impedance data with an equivalent circuit model of the lens. (**A**) The surface cell membrane conductance normalized to a unit area of lens surface. (**B**) The fiber cell membrane conductance per area of fiber cell membrane. (**C**) The effective extracellular resistivity, which depends on the volume fraction and tortuosity of the extracellular spaces within the lens. (**D**) The input resistance. The input resistance depends on size, specific membrane conductances, and the effective resistivity of the extracellular spaces within the lens. Many of these parameters are changing with age, leading to no systematic overall effect. The *dashed lines* in all of the panels are our arbitrary assessment of the general trend of age-dependent changes in each parameter.

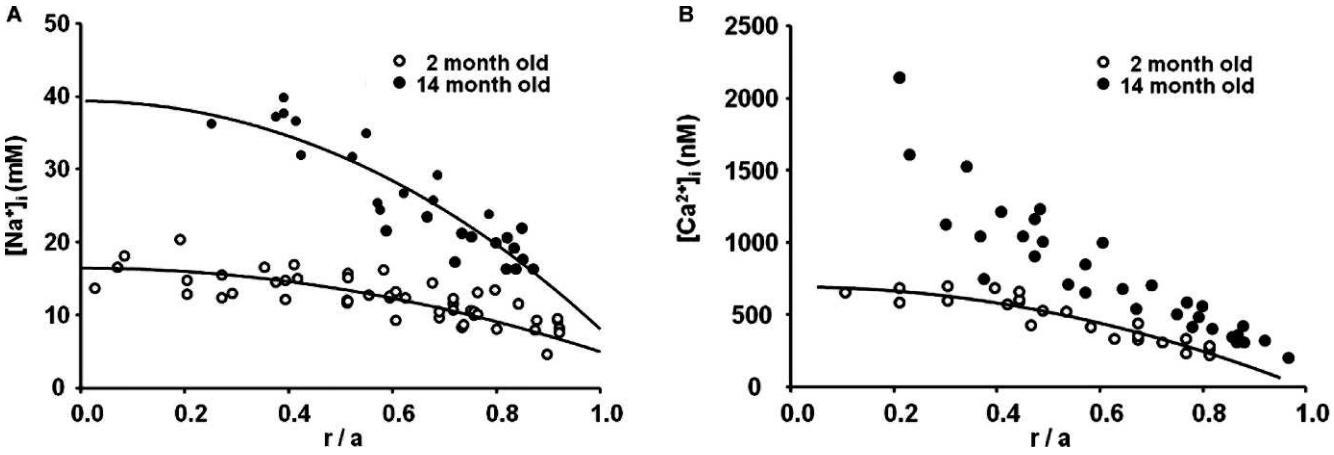


FIGURE 9. The effects of age on intracellular ion concentrations. (**A**) The intracellular sodium concentration graphed as a function of fractional distance from the lens center. At age 14 months, there is a much larger center to surface concentration gradient than at 2 months, due in part to the larger size and lower gap junction coupling conductance, but moderated by the reduced sodium influx. Both data sets are well fit by parabolic curves that indicate there is a continuous circulation of sodium between the center and surface of the lens. (**B**) The intracellular calcium concentration graphed as a function of fractional distance from the lens center. At age 14 months, there is a much larger center to surface concentration gradient than at 2 months. The data at age 2 months are well fit by a parabolic curve, which is based on a circulation of calcium between the lens center and surface. However, at age 14 months, the data no longer fall along such a curve, suggesting calcium influx across fiber cell membrane exceeds the rate of flow to the lens surface so there is uncontrolled accumulation in central fiber cells.

dashed line represents our interpretation of age effects on $G_S$ in adult mouse lenses. Figure 8B is the age-dependence of the fiber cell membrane conductance, $g_m$ ($S/cm^2$), referred to a unit area of fiber cell membrane. There is no systematic change in $g_m$ with age, so given the standard deviations in the data, the time-independent, flat dashed line represents our interpretation of age effects on $g_m$. Figure 8C shows the age dependence of the effective resistivity of the extracellular spaces within the lens, $R_e$ ($\Omega \cdot cm$), which depends on the tortuosity and volume fraction of the extracellular spaces.[29] The resistivity shows a large systematic increase with age that is essentially linear. This could be due to compaction of the extracellular spaces, at least in part due to the increased intracellular hydrostatic pressure with age, though the relative changes in resistivity are greater than those in hydrostatic pressure.

Figure 8D shows the age dependence of the lens input resistance, $R_{in}$ ($K\Omega$) (defined in Fig. 6A), which depends on lens size, specific membrane conductances of fiber and surface cells, and the effective resistivity of the extracellular spaces. As size increases, the input resistance was expected to decline owing to more membrane area, but increases in the effective extracellular resistivity appear to offset this decline, at least at ages 2 months and older, and there is no obvious systematic change in $R_{in}$ with the age of adult lenses. The decrease in $R_{in}$ between birth and age 2 months is probably the result of the relatively large growth during this early period, whereas there is surprisingly little change in adult lenses even though the lens continued to grow, albeit much more slowly than in the initial 2 months following birth.

The age-dependent changes in transport properties reported here presumably have some role in the changes in water flow velocity, sodium influx, and homeostasis of other ions involved in the lens circulation. The final set of experiments examined age-dependent effects on homeostasis of intracellular ions, with particular interest in $[Na^+]_i$, since it is an important factor in fiber cell transmembrane sodium influx and thus the lens circulation, and $[Ca^{2+}]_i$, since it is an important factor in cataractogenesis.

## The Effect of Age on Intracellular Ion Concentrations

Figure 9A shows the intracellular sodium concentrations at the ages of 2 and 14 months, graphed as a function of fractional distance from the lens center. The center to surface gradient is present to drive diffusion of sodium that enters fiber cells within the lens to surface cells where the Na/K ATPase can transport it out of the lens. In addition to intracellular diffusion of sodium from the lens center to surface, the flux of sodium is also carried by advection and conduction. In the older lenses, both advection and conduction have decreased, so diffusion has become relatively more important. However, there is also a decrease in sodium entry, but the large decrease in gap junction coupling conductance in connection with the increase in the relative role of diffusion have combined to cause a significant increase in the center-to-surface sodium gradient in the older lenses. The data at either age were adequately fit with a structurally based model of the lens circulation,[45] so the circulation of sodium appears to persist in the older lenses, but the gradient needed to generate the circulation has increased, leading to decreases in the fiber cell transmembrane electrochemical potential for sodium.

Figure 9B shows the distribution of intracellular calcium concentrations in lenses at age 2 and 14 months, graphed as a function of the fractional distance from the lens center. Calcium circulates through the lens in the same manner as sodium, but the intracellular concentration is so small that—unlike sodium, which drives the circulation of fluid and creates radial voltage gradients—it is a negligible factor in the circulation of fluid or in the voltage gradients. However, both fluid flow and voltage gradients contribute to the movement of intracellular calcium between the lens center and surface. Both of these factors are reduced in the older lenses, so diffusion becomes relatively more important, but the reduction in gap junction coupling conductance with age makes diffusion more difficult and requires a larger surface-to-center concentration gradient. The data at age 2 months are well fit with a structurally based model of the circulation[45]; however, by age 14 months, one can see that the parabolic concentration distribution is not present, so intracellular calcium is entering

Table 4. A Comparison of the Effects of Age Versus Species on Lens Transport Parameters.

| | $a$, cm | $G_{DF}$, S/cm² | $G_{MF}$, S/cm² | $p_i$, mm HG | $[Na^+]_i$, mM | $\psi_i$, mV | $R_e$, KΩ cm | $g_m$, μS/cm² | $j_{Na}$, moles/cm²s |
|---|---|---|---|---|---|---|---|---|---|
| Rat, 22 mo | 0.22 | 0.83 | 0.52 | 250 | 13 | −47 | 28 | 2 | 0.8 |
| Mouse, 2 mo | 0.11 | 0.93 | 0.82 | 250 | 13 | −47 | 27 | 4 | 3.5 |
| Mouse, 14 mo | 0.13 | 0.25 | 0.24 | 355 | 32 | −15 | 64 | 3 | 0.8 |

Mouse lens parameters were taken from the current study, whereas rat parameters were reported in Gao et al.[47] Average values of $p_i$, $[Na^+]_i$ and $\psi_i$ were obtained from the curve-fits at $r/a = 0.5$.

fiber cells more rapidly than it is circulating back to the surface for extrusion, hence it has begun to uncontrollably accumulate in central fiber cells.

## Discussion

The data presented here show that the process of aging has major effects on lens transport and homeostasis. A central factor in all these age-dependent changes is reduction in fiber cell gap junction coupling conductance. The coupling conductance data indicate that 14-month-old lenses have approximately a 70% reduction in coupling in either the DF or MF relative to 2-month-old lenses. This suggests the damage occurs in both domains. The Western blots are consistent with this interpretation, as the Cx46 antibody to the C-terminus shows loss of labeling in the DF, whereas the Cx50 antibody to the cytoplasmic loop shows loss of Cx50 labeling in the total lens. The DF eventually becomes MF; but in the old lenses, this process has greatly slowed relative to the rate of reduction in coupling conductance, which most probably is occurring throughout the lens. Coupling conductance, Cx46 labeling, and Cx50 labeling all go down with age at the same rate, suggesting degradation of connexin protein rather than a specific change in antibody labeling. However, we obviously do not know exactly what is happening to these proteins as the lens ages.

As coupling conductance decreased, the forces that drive the lens circulation had to increase to maintain the circulating fluxes. This included increases in the intracellular hydrostatic pressure gradient, diffusion gradient for sodium, and voltage gradient. However, these gradients did not increase as much as expected because the changes appear to be self-limiting. Both the accumulation of intracellular sodium and depolarization of the intracellular voltage with age led to a reduction in the fiber cell transmembrane electrochemical potential for sodium entry. Consequently, sodium influx decreased and since it drives water flow, water flow also decreased, thus moderating the increase in gradients for intracellular sodium concentration, voltage, and hydrostatic pressure.

The above-described changes affect intracellular calcium homeostasis, which is eventually lost in old lenses. Calcium appears to not permeate gap junctions as well as sodium (Fig. 9 and Wang et al.[45]), so the age-dependent reduction in gap junction–coupling conductance has a more significant effect on calcium than sodium. In normal young lenses, calcium circulates in the same manner as sodium; but if gap junction coupling is lost, as in the Cx46 knockout lenses, the egress path to the lens surface is blocked and calcium that enters through fiber cell membranes accumulates in the lens center.[44] In mouse lenses, calpain activity is initiated causing cleavage and aggregation of intracellular proteins[55,56] and a central cataract. Similarly, in old lenses, the egress pathway is compromised, so calcium entry through fiber cell membranes exceeds the rate of flow to the surface where it can be actively transported out of the lens. As a consequence, one can see in Figure 9B that intracellular calcium significantly accumulates in central fiber cells. A major difference between this situation and the Cx46 knockout lenses is that calpain activity decreases with age,[57,58] so the relatively high intracellular calcium concentration at age 14 months is not as devastating as it is in the knockout lenses, where calcium is similarly elevated at a young age. Nevertheless, uncontrolled accumulation of intracellular calcium can adversely affect many cellular processes, including activation of the remaining calpain. All of the lenses we studied at age 14 months were transparent, but normal mouse lenses do eventually get age-related nuclear cataracts,[59] and age-dependent loss of calcium homeostasis is probably an important factor.

### Effects of Lens Size/Age

Gao et al.[47] investigated the effect of lens size on the circulation of fluid and intracellular hydrostatic pressure in lenses from different species. The theoretical prediction was that, with other factors equal, intracellular hydrostatic pressure should increase as the radius squared ($a^2$). However, the "other factors" included a direct dependence on the average fiber cell membrane sodium influx ($j_{Na}$) and an inverse dependence on the number of open gap junction channels ($N_{MF}$), both of which could vary with species. They studied lenses from mice, rats, rabbits, and dogs with radii varying from 0.11 to 0.56 cm. Surprisingly, the central hydrostatic pressures were the same in these lenses of very different radii from different species. Further investigation of lenses from mice and rats suggested gap junction coupling, the effective extracellular resistivity, and the fiber cell transmembrane electrochemical potential for sodium were the same in the two types of lenses, but the fiber cell membrane conductance for sodium appeared to be lower in rat than mouse (see Table 4). The consequence was that sodium influx across fiber cell membranes decreased in larger lenses, leading to no difference in intracellular hydrostatic pressure at the center of the lenses.

The data presented here show that sodium influx across fiber cell membranes also decreases as the lens grows larger with age, but the mechanism appears to be entirely different. There was no systematic age-dependent change in the fiber cell membrane conductance, whereas the effective extracellular resistivity increased as the lens grew larger with age, but both gap junction–coupling conductance and the transmembrane electrochemical potential for sodium decreased (see Table 4). Hence, when size changed because of age, the pattern of physiological changes was opposite to that when size changed because of species.

Gao et al.[47] hypothesized that the species-dependent increase in lens size was associated with a species-dependent reduction in expression of sodium leak channels in fiber cells. They further hypothesized the purpose was to maintain a size-independent central hydrostatic pressure, which generated the radial gradient in refractive index. In the current study, we find the age-dependent increase in size and decrease in gap junction coupling conductance are associated with an intrinsic feedback mechanism that moderates the effects of these factors on the central intracellular hydrostatic pressure. The

expectation is the central intracellular pressure depends on $a^2 j_{Na}/N_{MF}$.[36,47] If $j_{Na}$ had not changed with age, the central hydrostatic pressure would have increased 5-fold between the ages of 2 and 14 months. Instead, the central hydrostatic pressure only increased approximately 1.4-fold, so the pressure data suggest a significant decrease in $j_{Na}$ over that time period. Based on independent measurements of the lens voltage and gap junction–coupling conductance, the estimate was that $j_{Na}$ decreased approximately 4-fold, consistent with the pressure data.

There was no detectable systematic change in fiber cell membrane conductance, so the decrease in $j_{Na}$ is probably due to a decrease in the average fiber cell transmembrane electrochemical potential for sodium ($\psi_i - \psi_e - E_{Na}$). Is this a feasible hypothesis? We have measured $\psi_i$ and $[Na^+]_i$. Assume the average values are close to the measured values at $r/a = 0.5$. At age 2 months, this gives $[Na^+]_i \approx 13$ mM and $\psi_i \approx -47$ mV. But to estimate the change in electrochemical potential, we have to estimate the values of $\psi_e$ and $[Na^+]_e$. Educated guesses at average values are $[Na^+]_e \approx 140$ mM and $\psi_e \approx -25$ mV,[31] so the average transmembrane electrochemical potential for fiber cell sodium is on the order of −84 mV. At age 14 months, the average intracellular values are around $[Na^+]_i \approx 35$ mM and $\psi_i \approx -15$ mV. With regard to the extracellular values, the circulating sodium current has decreased, but the effective extracellular resistivity has increased, so the sodium concentration and voltage have probably not changed much. With this assumption, at age 14 months, the average transmembrane electrochemical potential for fiber cell sodium is on the order of −26 mV, or more than a 3-fold decrease, which is reasonably consistent with the estimated decrease in $j_{Na}$.

Thus, quantitative estimates suggest experimentally observed changes between ages 2 and 14 months are interrelated in a self-consistent manner. Intrinsic feedback through age-dependent changes in intracellular sodium and voltage reduce sodium influx in older lenses and moderate hydrostatic pressure changes that would otherwise occur. Simple and approximate calculations like those above suggest the change in sodium concentration is approximately what would be expected from the decrease in gap junction coupling conductance, increased size, and the reduced sodium entry. The depolarization of the intracellular voltage, however, is greater than expected,[31] so there may indeed be other regulatory factors involved.

## Newborn Pup Lenses

When this study was initiated, we decided to look at mouse lenses from birth to old age to document systematic changes that might lead to age-related nuclear cataracts. The changes in transport parameters from 2 to 14 months followed the sort of slow changes that we were expecting, but the newborn pup lenses were unique in several unexpected ways.

First, the coupling conductance between mature fiber cells was remarkably large. To put this in perspective, at the nexus between heart cells, the conductance per area of cell-to-cell contact is approximately 0.33 S/cm$^2$.[60] In the zone of differentiating fiber cells of the young adult lens, the value is approximately 1 S/cm$^2$,[30] which is by far the highest reported conductance we had previously seen. The coupling conductance between mature fiber cells in the newborn pup lenses was an unprecedented 27 S/cm$^2$. This observation is intrinsically interesting, but it is probably not due to the processes that led to the continuous reduction in coupling that is seen from 2 to 14 months. We suspect the huge coupling conductance in pups is more related to growth factors and other hormones that are present during this initial phase of rapid growth,[61] whereas the subsequent slow decline in coupling conductance in adult lenses (2–14 months) is due to accumulation of oxidative damage to gap junction channels.[45]

How and why is the coupling conductance that high? We can think of two possibilities on how, but have no specific idea on why such a high conductance is required.

First, with regard to how, these young lenses could have many cell-to-cell fusions,[62–64] which would be indistinguishable from gap junction connections in our electrical experiments. This idea, however, makes the hydrostatic pressure measurements more difficult to understand. Fusions would have a much lower cell-to-cell hydraulic conductance, which depends on the fourth power of the pore radius, than many smaller gap junction channels, so the pressure gradient should have been anomalously low. However, the experimentally measured pressure gradient is higher than expected based on the assumption that gap junctions mediate both ion and fluid flow. If the relationship $p_f(0) - p_f(b) \propto b^2 j_{Na}/N_{MF}$ is used to predict changes in the pressure gradient, then the gradient at 2 to 3 days should have been 1% of that at 2 months, or around 4 mm Hg, whereas the experimental gradient is 42 mm Hg. This discrepancy is discussed below, but it would be more difficult to explain if fusions generated the high conductance.

Alternatively, the gap junction literature contains many references to what is termed a "latent" pool of channels.[65,66] This pool is observed when one measures the single cell-to-cell channel conductance and also estimates the number of cell to cell channels, then the predicted cell-to-cell conductance is always much larger than the measured conductance, and this is true in the lens. In the lens, the area of gap junction plaques per area of cell-to-cell contact varies with location, but in the outer cortex of the chick lens, the estimate is 33.7%.[67] For comparison, at the intercalated disc in the cardiac ventricle of rats, the density is estimated at 23%.[68] Zampighi et al.[69] estimate the channel density of a gap junction plaque in the lens cortex to be 10,952/μm$^2$, or approximately a 9-nm channel to channel spacing, a number consistent with many other estimates of channel packing within plaques. Channels made from Cx46 and Cx50, respectively, have single channel conductances of 140 pS and 210 pS,[70,71] so the average is approximately 175 pS. These numbers suggest the coupling conductance per area of cell-to-cell contact could be as high as 50 S/cm$^2$, which, given our DF conductance measurements in 2-month-old mouse lenses, implies only approximately 1 channel in 50 is open. In the lenses from newborn pups, there could be some signal that opens these "latent" channels for some unknown purpose. The measured cell-to-cell coupling conductance is in reasonable agreement with the number of channels, so this is our best guess, but more specific hypotheses will require a great deal more work.

The second anomaly is the spatial distribution of coupling conductance. In frog, rat, and mouse lenses, the DF to MF transition occurs at $r = 0.85a$, where the MF loses organelles, and cleavage of most membrane proteins occurs. There is a reduction in coupling conductance at the DF to MF transition, probably due to cleavage of the C-terminus of Cx50 channels,[30] which causes them to have a greatly reduced open probability.[72] In lenses from newborn pups, the pattern is reversed and the coupling conductance of DF is much lower than that of MF. The reason could be as simple as rapid growth exceeding the rate of assembly of junctional plaques, but this should not give an abrupt change in slope at $r = 0.85a$, which is coincidental with the DF to MF transition. The abruptness of the change in slope and the sudden large coupling conductance look more like a programmed event, due to post-translational modifications of the gap junction channels, but its purpose is unknown.

The third anomaly is the intracellular hydrostatic pressure gradient, which was mentioned above. Given the remarkably

high coupling conductance of MF, a very low central intracellular hydrostatic pressure should have been sufficient to drive intracellular water flow, unless the flow velocity was exceptionally large, which was not the case (see Table 2). Hence, the central pressure should have been an order of magnitude lower than measured. In contrast, the voltage gradient shown in Figure 7 is essentially flat, consistent with the large coupling conductance. The prediction that the central pressure should be proportional to $a^2 j_{Na}/N_{MF}$ appears to hold for the adult lenses studied either here or by Gao et al.,[36,47] but it does not hold for the lenses from newborn pups. The value of $N_{MF}$ in this relationship is based on coupling conductance, with the assumption that single gap junction channel ionic or hydraulic conductances are not changing. Though it seems unlikely, perhaps the single channel ratio of hydraulic to ionic conductance is lower in gap junction channels in lenses from newborn pups than in lenses from adult mice, or perhaps the large coupling conductance in pup lenses is due to some factor other than gap junctions, a factor that does not add much hydraulic conductivity. These thoughts, however, are rather vague. A more physically based idea is that electroosmosis drives a large fraction of water flow through gap junctions in adult lenses, where there is a significant radial gradient in voltage,[36] thus reducing the pressure gradient needed to keep all the fluid moving. But in pup lenses, the voltage gradient is absent, thus pressure is the only factor that drives fluid flow. For roughly the same fluid flow, the lens would require a much larger pressure gradient in the absence of a voltage gradient.[73]

## Summary

The central observation in this paper is the age-dependent reduction in gap junction coupling conductance, which follows the reduction in Cx46 and Cx50 labeling seen in Western blots. Based on previous work,[45] our working hypothesis is that fiber cell connexins are particularly sensitive to oxidative damage, though we have no data on whether this is a direct effect or occurs indirectly through some stress-activated pathway that leads to connexin degradation. Down-regulation of gap junction coupling as well as increases in size with age cause depolarization of the intracellular voltage, and increases in intracellular concentrations of both sodium and calcium. Increased intracellular calcium concentration can adversely affect many intracellular homeostatic mechanisms, while depolarization and increased intracellular sodium concentration reduce the transmembrane driving force for fiber cell membrane sodium-dependent transporters, which are also responsible for intracellular homeostasis.[29] Altogether, these effects may compromise systems that protect intracellular proteins and allow increased oxidative damage to crystallins and their consequent aggregation, which leads to light scattering. Thus, a pharmacological means of increasing gap junction coupling in the lens might significantly delay the onset of age-related nuclear cataracts. Interestingly, some factors, possibly growth factors,[74] may indeed greatly increase gap junction coupling in lenses from newborn pups, so if those factors could be identified, they might lead to a pharmacological solution for cataracts.

## *Acknowledgments*

Supported by grants from the National Institutes of Health through the National Eye Institute: EY06391, EY13163, and EY20506.

Disclosure: **J. Gao**, None; **H. Wang**, None; **X. Sun**, None; **K. Varadaraj**, None; **L. Li**, None; **T.W. White**, None; **R.T. Mathias**, None

## *References*

1. Leading cause of blindness. *NIH Medline Plus*. 2008;3:14–15.
2. Berry V, Mackay D, Khaliq S, et al. Connexin 50 mutation in a family with congenital "zonular nuclear" pulverulent cataract of Pakistani origin. *Hum Genet*. 1999;105:168–70.
3. Mackay D, Ionides A, Kibar Z, et al. Connexin46 mutations in autosomal dominant congenital cataract. *Am J Hum Genet*. 1999;64:1357–64.
4. Shiels A, Bassnett S. Mutations in the founder of the MIP gene family underlie cataract development in the mouse. *Nat Genet*. 1996;12:212–215.
5. Spector A. Oxidative stress-induced cataract: mechanism of action. *FASEB J*. 1995;9:1173–1182.
6. Dovrat A, Weinreb O. Effects of UV-A radiation on lens epithelial NaK-ATPase in organ culture. *Invest Ophthalmol Vis Sci*. 1999;40:1616–1620.
7. Truscott RJ. Human cataract: the mechanisms responsible; light and butterfly eyes. *Int J Biochem Cell Biol*. 2003;35:1500–1504.
8. Giblin FJ, Leverenz VR, Padgaonkar VA, et al. UVA light in vivo reaches the nucleus of the guinea pig lens and produces deleterious, oxidative effects. *Exp Eye Res*. 2002;75:445–458.
9. Reddy VN, Giblin FJ, Lin LR, et al. Glutathione peroxidase-1 deficiency leads to increased nuclear light scattering, membrane damage, and cataract formation in gene-knockout mice. *Invest Ophthalmol Vis Sci*. 2001;42:3247–3255.
10. Garner WH, Garner MH, Spector A. H2O2-induced uncoupling of bovine lens Na+, K+-ATPase. *Proc Natl Acad Sci U S A*. 1983;80:2044–2048.
11. Garner MH, Garner WH, Spector A. H2O2-modification of Na, K-ATPase. Alterations in external Na+ and K+ stimulation of K+ influx. *Invest Ophthalmol Vis Sci*. 1986;27:103–107.
12. McNulty R, Wang H, Mathias RT, Ortwerth BJ, Truscott RJ, Bassnett S. Regulation of tissue oxygen levels in the mammalian lens. *J Physiol*. 2004;559(pt 3):883–898.
13. Padgaonkar VA, Leverenz VR, Fowler KE, Reddy VN, Giblin FJ. The effects of hyperbaric oxygen on the crystallins of cultured rabbit lenses: a possible catalytic role for copper. *Exp Eye Res*. 2000;71:371–383.
14. Borchman D, Giblin FJ, Leverenz VR, et al. Impact of aging and hyperbaric oxygen in vivo on guinea pig lens lipids and nuclear light scatter. *Invest Ophthalmol Vis Sci*. 2000;41:3061–3073.
15. Bron AJ, Vrensen GF, Koretz J, Maraini G, Harding JJ. The ageing lens. *Ophthalmologica*. 2000;214:86–104.
16. Horwitz J. Proctor Lecture. The function of alpha-crystallin. *Invest Ophthalmol Vis Sci*. 1993;34:10–22.
17. Paterson CA, Zeng J, Husseini Z, et al. Calcium ATPase activity and membrane structure in clear and cataractous human lenses. *Curr Eye Res*. 1997;16:333–338.
18. Truscott RJ, Martinez MG. Decolouration of the lens pigment in senile nuclear cataract. *Ophthalmic Res*. 1990;22:241–246.
19. Menko AS. Lens epithelial cell differentiation. *Exp Eye Res*. 2002;75:485–490.
20. Zampighi GA, Eskandari S, Kreman M. Epithelial organization of the mammalian lens. *Exp Eye Res*. 2000;71:415–435.
21. Griep AE, Zhang P. Lens cell proliferation. In: Lovicu FJ, Robinson ML, eds. *Development of the Ocular Lens*. Cambridge, UK: Cambridge University Press; 2004:191–213.
22. Candia OA, Zamudio AC. Regional distribution of the Na(+) and K(+) currents around the crystalline lens of rabbit. *Am J Physiol Cell Physiol*. 2002;282:C252–C262.
23. Baldo GJ, Mathias RT. Spatial variation in membrane properties in the intact rat lens. *Biophys J*. 1992;68:518–529.

24. Le AC, Musil LS. Normal differentiation of cultured lens cells after inhibition of gap junction-mediated intercellular communication. *Dev Biol*. 1998;204:80–96.
25. Boswell BA, Overbeek PA, Musil LS. Essential role of BMPs in FGF-induced secondary lens fiber differentiation. *Dev Biol*. 2008;324:202–212.
26. Bassnett S, Beebe DC. Coincident loss of mitochondria and nuclei during lens fiber cell differentiation. *Dev Dyn*. 1992; 194:85–93.
27. Kistler J, Bullivant S. Protein processing in lens intercellular junctions: cleavage of MP70 to MP38. *Invest Ophthalmol Vis Sci*. 1987;28:1687–192.
28. Jacobs MD, Soeller C, Sisley AM, Cannell MB, Donaldson PJ. Gap junction processing and redistribution revealed by quantitative optical measurements of connexin46 epitopes in the lens. *Invest Ophthalmol Vis Sci*. 2004;45:191–199.
29. Mathias RT, Kistler J, Donaldson P. The lens circulation. *J Membr Biol*. 2007;216:1–16.
30. Mathias RT, White TW, Gong X. Lens gap junctions in growth, differentiation, and homeostasis. *Physiol Rev*. 2010;90:179–206.
31. Mathias RT, Rae JL, Baldo GJ. Physiological properties of the normal lens. *Physiol Rev*. 1997;77:21–50.
32. Vaghefi E, Walker K, Pontre BP, Jacobs MD, Donaldson PJ. Magnetic resonance and confocal imaging of solute penetration into the lens reveals a zone of restricted extracellular space diffusion. *Am J Physiol Regul Integr Comp Physiol*. 2012;302:R1250–R1259.
33. Gao J, Sun X, Yatsula V, Wymore RS, Mathias RT. Isoform specific function and distribution of Na/K pumps in the frog lens epithelium. *J Mem Biol*. 2000;178:89–101.
34. Tamiya S, Dean WL, Paterson CA, Delamere NA. Regional distribution of Na, K-ATPase activity in porcine lens epithelium. *Invest Ophthalmol Vis Sci*. 2003;44:4395.
35. Vaghefi E, Pontre BP, Jacobs MD, Donaldson PJ. Visualizing ocular lens fluid dynamics using MRI: manipulation of steady state water content and water fluxes. *Am J Physiol Regul Integr Comp Physiol*. 2011;301:R335–R342.
36. Gao J, Sun X, Moore LC, White TW, Brink PR, Mathias RT. Lens intracellular hydrostatic pressure is generated by the circulation of sodium and modulated by gap junction coupling. *J Gen Physiol*. 2011;137:507–520.
37. Candia OA, Mathias R, Gerometta R. Fluid circulation determined in the isolated bovine lens. *Invest Ophthalmol Vis Sci*. 2012;53:7087–7096.
38. Merriman-Smith BR, Krushinsky A, Kistler J, Donaldson PJ. Expression patterns for glucose transporters GLUT1 and GLUT3 in the normal rat lens and in models of diabetic cataract. *Invest Ophthalmol Vis Sci*. 2003;44:3458–3466.
39. Merriman-Smith R, Donaldson P, Kistler J. Differential expression of facilitative glucose transporters GLUT1 and GLUT3 in the lens. *Invest Ophthalmol Vis Sci*. 1999;40:3224–3330.
40. Li L, Lim JC, Jacobs MD, Kistler J, Donaldson PJ. Regional differences in cystine accumulation point to a sutural delivery pathway to the lens core. *Invest Ophthalmol Vis Sci*. 2007;48: 1253–1260.
41. Lim J, Lam YC, Kistler J, Donaldson PJ. Molecular characterization of the cystine/glutamate exchanger and the excitatory amino acid transporters in the rat lens. *Invest Ophthalmol Vis Sci*. 2005;46:2869–2877.
42. Lim J, Lorentzen KA, Kistler J, Donaldson PJ. Molecular identification and characterization of the glycine transporter (GLYT1) and the glutamine/glutamate transporter (ASCT2) in the rat lens. *Exp Eye Res*. 2006;83:447–455.
43. Gong X, Li E, Klier G, et al. Disruption of alpha3 connexin gene leads to proteolysis and cataractogenesis in mice. *Cell*. 1997;91:833–843.
44. Gao J, Sun X, Martinez-Wittinghan FJ, Gong X, White TW, Mathias RT. Connections between connexins, calcium, and cataracts in the lens. *J Gen Physiol*. 2004;124:289–300.
45. Wang H, Gao J, Sun X, et al. The effects of GPX-1 knockout on membrane transport and intracellular homeostasis in the lens. *J Membr Biol*. 2009;227:25–37.
46. White TW, Goodenough DA, Paul DL. Targeted ablation of connexin50 in mice results in microphthalmia and zonular pulverulent cataracts. *J Cell Biol*. 1998;143:815–825.
47. Gao J, Sun X, Moore LC, Brink PR, White TW, Mathias RT. The effect of size and species on lens intracellular hydrostatic pressure. *Invest Ophthalmol Vis Sci*. 2013;54:183–192.
48. Eisenberg RS, Barcilon V, Mathias RT. Electrical properties of spherical syncytia. *Biophys J*. 1979;25:151–180.
49. Mathias RT, Rae JL, Eisenberg RS. The lens as a nonuniform spherical syncytium. *Biophys J*. 1981;34:61–83.
50. Paul DL, Ebihara L, Takemoto LJ, Swenson KI, Goodenough DA. Connexin46, a novel lens gap junction protein, induces voltage-gated currents in nonjunctional plasma membrane of Xenopus oocytes. *J Cell Biol*. 1991;115:1077–1089.
51. Gong X, Baldo GJ, Kumar NM, Gilula NB, Mathias RT. Gap junctional coupling in lenses lacking alpha3 connexin. *Proc Natl Acad Sci U S A*. 1998;95:15303–15308.
52. Baldo GJ, Gong X, Martinez-Wittinghan FJ, Kumar NM, Gilula NB, Mathias RT. Gap junctional coupling in lenses from alpha(8) connexin knockout mice. *J Gen Physiol*. 2001;118: 447–456.
53. Mathias RT, Wang H. Local osmosis and isotonic transport. *J Membr Biol*. 2005;208:39–53.
54. Wang J, Ma M, Locovei S, Keane RW, Dahl G. Modulation of membrane channel currents by gap junction protein mimetic peptides: size matters. *Am J Physiol Cell Physiol*. 2007;293: C1112–C1119.
55. Baruch A, Greenbaum D, Levy ET, et al. Defining a link between gap junction communication, proteolysis, and cataract formation. *J Biol Chem*. 2001;276:28999–9006.
56. Tang Y, Liu X, Zoltoski RK, et al. Age-related cataracts in alpha3Cx46-knockout mice are dependent on a calpain 3 isoform. *Invest Ophthalmol Vis Sci*. 2007;48:2685–2694.
57. Reed NA, Castellini MA, Ma H, Shearer TR, Duncan MK. Protein expression patterns for ubiquitous and tissue specific calpains in the developing mouse lens. *Exp Eye Res*. 2003;76: 433–443.
58. Ma H, Shih M, Fukiage C, et al. Influence of specific regions in Lp82 calpain on protein stability, activity, and localization within lens. *Invest Ophthalmol Vis Sci*. 2000;41:4232–4239.
59. Reddy VN, Giblin FJ, Lin LR, et al. Glutathione peroxidase-1 deficiency leads to increased nuclear light scattering, membrane damage, and cataract formation in gene-knockout mice. *Invest Ophthalmol Vis Sci*. 2001;42:3247–3255.
60. Weidmann S, Hodgkin AI. The diffusion of radiopotassium across interrelated disks of mammalian cardiac muscle. *J Physiol Lond*. 1966;187:323–342.
61. Lang RA, McAvoy JW. Growth factors in lens development. In: Lovicu FJ, Robinson ML, eds. *Development of the Ocular Lens*. Cambridge, UK: Cambridge University Press; 2004:261–290.
62. Kuszak JR, Macsai MS, Bloom KJ, Rae JL, Weinstein RS. Cell-to-cell fusion of lens fiber cells in situ: correlative light, scanning electron microscopic, and freeze-fracture studies. *J Ultrastruct Res*. 1985;93:144–160.
63. Shi Y, Barton K, De Maria A, Petrash JM, Shiels A, Bassnett S. The stratified syncytium of the vertebrate lens. *J Cell Sci*. 2009; 122(pt 10):1607–1615.
64. Shi Y, De Maria AB, Wang H, Mathias RT, FitzGerald PG, Bassnett S. Further analysis of the lens phenotype in Lim2-deficient mice. *Invest Ophthalmol Vis Sci*. 2011;52:7332–7339.


Investigative Ophthalmology & Visual Science

65. Bukauskas FF, Jordan K, Bukauskiene A, et al. Clustering of connexin 43-enhanced green fluorescent protein gap junction channels and functional coupling in living cells. *Proc Natl Acad Sci U S A*. 2000;97:2556–2661.
66. Palacios-Prado N, Bukauskas FF. Modulation of metabolic communication through gap junction channels by transjunctional voltage; synergistic and antagonistic effects of gating and ionophoresis. *Biochim Biophys Acta*. 2012;1818:1884–1894.
67. Biswas SK, Jiang JX, Lo WK. Gap junction remodeling associated with cholesterol redistribution during fiber cell maturation in the adult chicken lens. *Mol Vis*. 2009;15:1492–508.
68. Chen L, Goings GE, Upshaw-Earley J, Page E. Cardiac gap junctions and gap junction-associated vesicles: ultrastructural comparison of in situ negative staining with conventional positive staining. *Circ Res*. 1989;64:501–514.
69. Zampighi GA, Eskandari S, Hall JE, Zampighi L, Kreman M. Micro-domains of AQP0 in lens equatorial fibers. *Exp Eye Res*. 2002;75:505–519.
70. Hopperstad MG, Srinivas M, Spray DC. Properties of gap junction channels formed by Cx46 alone and in combination with Cx50. *Biophys J*. 2000;79:1954–1966.
71. Srinivas M, Costa M, Gao Y, Fort A, Fishman GI, Spray DC. Voltage dependence of macroscopic and unitary currents of gap junction channels formed by mouse connexin50 expressed in rat neuroblastoma cells. *J Physiol*. 1999;517(pt 3):673–689.
72. DeRosa AM, Xia CH, Gong X, White TW. The cataract-inducing S50P mutation in Cx50 dominantly alters the channel gating of wild-type lens connexins. *J Cell Sci*. 2007;120:4107–4116.
73. McLaughlin S, Mathias RT. Electro-osmosis and the reabsorption of fluid in renal proximal tubules. *J Gen Physiol*. 1985;85:699–728.
74. Boswell BA, Le AC, Musil LS. Upregulation and maintenance of gap junctional communication in lens cells. *Exp Eye Res*. 2009;88:919–927.

Investigative Ophthalmology & Visual Science